*Progress In Electromagnetics Research B, Vol. 88, 53–71, 2020*

# A Super Resolution and Highly Stable Technique for Direction of Arrival Estimation of Coherent Sources for mm-Wave Radars

**Amr H. Hussein[1, *], Mohamed H. Mabrouk[2], and Haythem H. Abdullah[3]**

**Abstract**—In this paper, a new super-resolution and highly stable DOA estimation technique of coherent sources is introduced. Furthermore, the proposed technique is applied to the data collected from the AWR1243 mm-wave 76–81 GHz frequency modulated continuous wave (FMCW) radar to estimate the DOAs of real targets. A virtual antenna array is proposed to increase the array aperture size and the dimension of the data covariance matrix which effectively helps in de-correlating the received signals and in increasing the number of detectable sources and hence improving the detection resolution. Moreover, a significant improvement in the DOA estimation capability is achieved by handling the frequency domain of the received signals instead of their time-domain representations. That is because the signal to noise ratio (SNR) is increased by a multiplication factor when it is transformed using FFT which acts as a filter for the noise. The simulation results proved the superiority of the proposed technique compared to the state of the arts in this field, especially at low SNR that approaches −35 dB.

## 1. INTRODUCTION

The direction of arrival (DOA) estimation of targets or sources is one of the most critical research issues in recent wireless communications especially for radar systems. Generally, the sources to be detected can be classified into coherent and non-coherent sources, where the existence of coherent sources arises from multipath propagation and man-made interference. The most commonly used signal subspace DOA estimation algorithms are: the MUSIC and the estimation of signal parameters via rotational invariance techniques (ESPRIT) algorithms. These algorithms are characterized by their high resolution and accuracy in the case of non-coherent sources and high SNR regimes. However, their performances are highly degraded in the case of coherent sources detection and low SNR [1–6]. Many research articles have been introduced to tackle this problem. As a solution, the spatial smoothing represented in forward spatial smoothing (SS) and forward-backward spatial smoothing (FBSS) has been introduced [7, 8]. An important benefit of performing spatial smoothing is the formation of sharper peaks in the spatial spectrums of the MUSIC and the ESPRIT algorithms, which results in high resolution.

For efficient coherent sources detection, signals decorrelation has to be performed before estimating the spatial spectrum of the intended DOA estimation algorithm. VAE has emerged as a promising solution for this purpose [9, 10]. VAE increases the array size from $M$ to $2M-1$ elements by employing the conjugate of the antenna array excitation coefficients around the reference antenna element. In this case, the number of virtual signals is increased allowing the algorithm to detect more sources. In [9], the modified VAE-SS based DOA estimation technique denoted as VSS is introduced. For further performance enhancement of coherent sources detection, SVD based DOA estimation algorithms has been introduced [11, 12]. In [11], the SVD of the received data covariance matrix is utilized to construct

*Received 29 May 2020, Accepted 12 August 2020, Scheduled 27 August 2020*
* Corresponding author: Amr Hussein Hussein Abdullah (amrvips@yahoo.com).
[1] Electronics and Electrical Communications Engineering Department, Faculty of Engineering, Tanta University, Tanta, Egypt.
[2] Electrical and Computer Engineering Department, Faculty of Engineering, Alexandria University, Alexandria, Egypt. [3] Electronics Research Institute, Joseph Tito St, Huckstep, Qism El-Nozha, Cairo Governorate, Egypt.

a new covariance matrix from the eigenvector corresponding to the largest eigenvalue. After that, the SVD is performed again on the new covariance matrix. However, it suffers poor performance at low SNR. In [12], a modified SVD algorithm is introduced to improve the performance of the traditional SVD based DOA algorithms. Based on the modified SVD and modified MUSIC algorithms introduced in [12] and [13], respectively, the high resolution MV-SVD DOA estimation algorithm has been introduced in [14]. In [15], a Maximum Likelihood (ML) method for DOA estimation based on an improved squirrel search algorithm (ISSA) has been introduced. It is introduced to minimize the complexity and search burden for optimal directions. The proposed technique using ISSA introduced better performance than the other optimization techniques such as seeker optimization algorithm (SOA), sine cosine algorithm (SCA), genetic algorithm (GA), particle swarm optimization (PSO) and differential evolution (DE). But, generally, the ML-ISSA DOA technique provided high root mean square error (RMSE) in between $10^1$ and $10^2$ at SNR $= -20$ dB. In [16], based on the principle of operation of the minimum norm (MN) algorithm, a low complexity and super-resolution DOA estimation algorithm has been introduced for an unknown number of sources. This MN-like algorithm has provided higher performance than the MUSIC-like DOA estimation algorithm introduced in [17]. However, they provide a low resolution and relatively high average RMSE at low SNR. As another solution, antenna arrays beamforming can add a valuable impact on the working DOA estimation techniques. In [18], a new linear antenna arrays synthesis technique using reduced number of antenna elements and its application to DOA estimation algorithms has been introduced. The synthesized array has nonuniform excitations and larger element spacing than the traditional uniform linear array (ULA) which reduces the coupling between the received signals impinging on the antenna array elements. The simulations revealed that the beamforming based DOA estimation technique has better performance than the other ULA based techniques.

In this paper, a new DOA estimation technique for coherent sources is proposed. The proposed technique applies an FFT algorithm to the output of the proposed virtual array distribution. The array is virtually extended to mimic the availability of double the existing number of array elements. The output of the FFT is limited to the signal spectrum by truncating a wide band of the noise spectrum. Consequently, the array extension increases the resolution while the utilization of the FFT enhances the SNR. Several simulation scenarios are carried to verify the superiority of the proposed technique compared to the other modern DOA estimation techniques such as FBSS [8], VSS [9], SVD [11], MV-SVD [14], and the array signal segregation using an iterative approach (ASSIA) combined with the closely-spaced nulls synthesis method (CNSM) that is denoted as the ASSIA-CNSM algorithm [25]. Multiple aspects of comparison were covered including the number of detectable sources, stability, mean square error, and angular resolution versus the signal to noise ratio. The proposed technique provides a resolution of 0.088 HPBW, where HPBW is the half power beamwidth of the antenna array. The rest of the paper is organized as follows. In Section 2, the proposed DOA estimation technique is introduced. In Section 3, the simulation results of the proposed technique and state of the art techniques are discussed. In Section 4, the application of the proposed technique for experimental DOA estimation using the data collected from the AWR1243 mm-wave 76–81 GHz FMCW transceiver is introduced. Finally, the paper is concluded in Section 5. The vectors and matrices are written in boldface.

## 2. PROPOSED DOA ESTIMATION TECHNIQUE

One of the most favorable techniques used in DOA estimation of coherent sources is the SVD as it achieves decorrelation of coherent signals. However, its performance is highly degraded at low SNR scenarios. In this section, the proposed DOA estimation technique is introduced. This technique provides not only a reliable DOA estimation with high resolution, but also with high stability, and larger number of detectable sources at very low SNR regimes. The proposed DOA estimation technique is shown in Fig. 1. Structurally, the FFT is applied for large number of samples $N$ to obtain a high spectral separation resolution. Further, to minimize the complexity and computational time of the covariance matrix, additional down sampling block is added to the block diagram after the $N$-point FFT to reduce the number of transformed signal samples from $N$ to $Q$ such that $Q \ll N$. Each block will be explained in the following four main steps:

***Step (1)***: In this step, the received signal model by applying VAE is introduced. For higher DOA resolution, the number of antennas should be increased to collect more signals information. But, due to

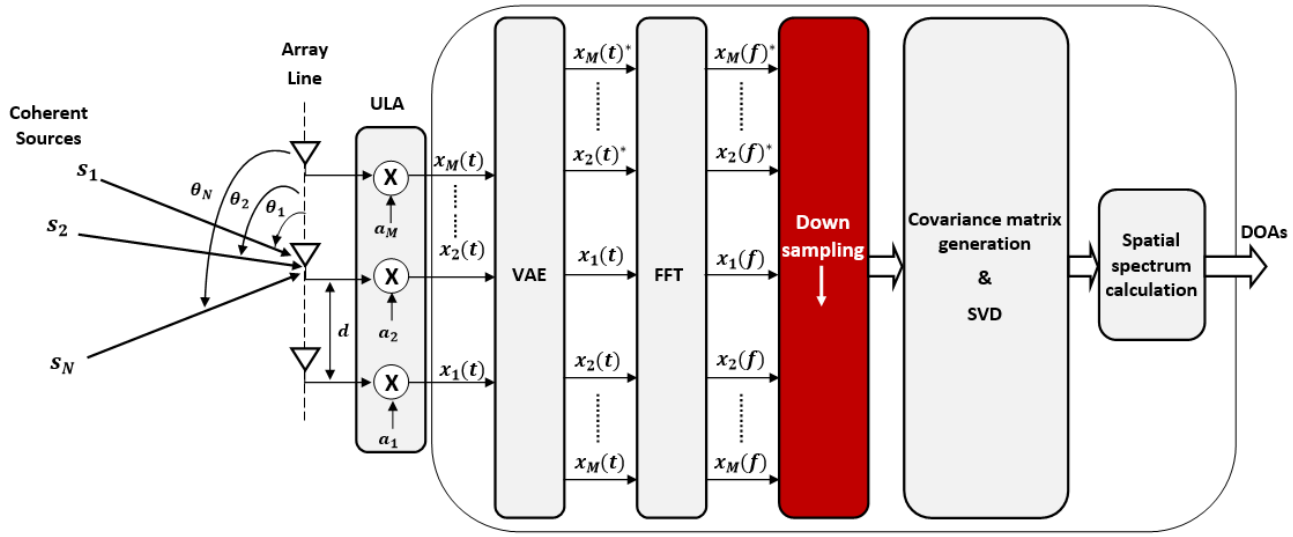


**Figure 1.** The block diagram of the proposed DOA estimation technique.

space and RF front end cost constraints, increasing the number of antenna elements is not preferable. To tackle this issue, VAE is used to increase the number of effective signal channels without changing the antenna array size [9]. The conventional DOA estimation systems are based on utilizing ULAs. The array factor $\mathbf{AF}(\theta)$ of a ULA consisting of $M$ antenna elements with uniform inter-element spacing $d$ is given by:

$$\mathbf{AF}(\theta) = \sum_{m=1}^{M} a_m e^{jk(m-1)d\cos\Theta} \tag{1}$$

where $a_m$ is the complex excitation coefficient of the $m$th antenna element, and $k = 2\pi/\lambda$ is the free space wave number at the carrier wavelength $\lambda$ [19]. Consider $N$ coherent or non-coherent signal sources radiating narrow band signals which are impinging on the ULA from the directions ($\theta_1$, $\theta_2$, ..., $\theta_N$) where ($N < M$), the received signal $\mathbf{X}(t)$ at the ULA elements is given by [1]:

$$\mathbf{X}(t) = \mathbf{AS}(t) + \mathbf{W}(t) \tag{2}$$

where

$$\begin{aligned} \mathbf{X}(t) &= [x_1(t)\ \ x_2(t)\ \ \ldots\ldots\ldots\ x_M(t)]^T \\ \mathbf{S}(t) &= [s_1(t)\ \ s_2(t)\ \ \ldots\ldots\ldots\ s_N(t)]^T \\ \mathbf{W}(t) &= [\omega_1(t)\ \ \omega_2(t)\ \ \ldots\ldots\ldots\ \omega_M(t)]^T \\ \mathbf{A} &= [\mathbf{a}(\theta_1)\ \ \mathbf{a}(\theta_2)\ \ \ldots\ldots\ldots\ \mathbf{a}(\theta_N)] \\ \mathbf{a}(\theta_n) &= \left[1\ e^{-jkd\cos\theta_n}\ \ldots\ e^{-jk(M-1)d\cos\theta_n}\right]^T \end{aligned} \tag{3}$$

where $x_m(t)$ is the received signal at the $m$th antenna element at any time instant $t$. $s_n(t)$ is the narrow band signal emitted from the $n$th source. $\omega_m(t)$ is the additive white gaussian noise (AWGN) with zero mean $\mu_\omega = 0$ and variance $\sigma_\omega^2$. $\mathbf{A}$ is the steering matrix of dimensions $(M \times N)$ and $\mathbf{a}(\theta_n)$ is the steering vector of dimensions $(M \times 1)$ for a specific source direction $\theta_n$ and taking the first antenna element as the reference. $[\cdot]^T$ is the matrix/vector transpose. The VAE is a technique that is used to extend the $M$-element ULA size from actual $M$ elements to a virtual $2M-1$ elements ULA as shown in Fig. 1. In this case, the $((2M-1)\times 1)$ steering vector of the virtual array $\mathbf{a_v}(\theta_n)$ at any source direction $\theta_n$ is given by:

$$\mathbf{a_v}(\theta_n) = \left[e^{jk(M-1)d\cos\theta_n}\ \ldots\ e^{jkd\cos\theta_n}\ 1\ e^{-jkd\cos\theta_n}\ \ldots\ e^{-jk(M-1)d\cos\theta_n}\right]^T \tag{4}$$

The corresponding $((2M-1)\times N)$ virtual array steering matrix $\mathbf{A_v}$ is given by:

$$\mathbf{A_v} = [\mathbf{a_v}(\theta_1)\ \ \mathbf{a_v}(\theta_2)\ \ \ldots\ldots\ldots\ \mathbf{a_v}(\theta_N)] \tag{5}$$

where the reference element is taken at the center of the virtual array. The $((2M-1)\times 1)$ virtually received signal vector $\mathbf{X_v}(t)$, the $((2N-1)\times 1)$ virtually transmitted signal vector $\mathbf{S_v}(t)$, and the $((2M-1)\times 1)$ virtually noise signal vector $\mathbf{W_v}(t)$ in the time domain are written as:

$$\begin{aligned}
\mathbf{X_v}(t) &= [x_M(t)^*\ \ldots\ldots\ldots\ x_2(t)^*\ x_1(t)\ x_2(t)\ \ldots\ldots\ldots\ x_M(t)]^T \\
\mathbf{S_v}(t) &= [s_N(t)^*\ \ldots\ldots\ldots\ s_2(t)^*\ s_1(t)\ s_2(t)\ \ldots\ldots\ldots\ s_N(t)]^T \\
\mathbf{W_v}(t) &= [\omega_M(t)^*\ \ldots\ldots\ldots\ \omega_2(t)^*\ \omega_1(t)\ \omega_2(t)\ \ldots\ldots\ldots\ \omega_M(t)]^T
\end{aligned} \tag{6}$$

The virtual received signal model is expressed as:

$$\mathbf{X_v}(t) = \mathbf{A_v}\mathbf{S_v}(t) + \mathbf{W_v}(t) \tag{7}$$

***Step (2)***: In this step,the fast Fourier transform (FFT) of the virtually received signal is performed, and its impact on the signal to noise ratio is analyzed. The discrete time representation of the virtual received signals at each antenna is expressed as:

$$\mathbf{X_v}(k), \quad k = 1,2,3,\ldots\ldots,K \tag{8}$$

where $K$ is the number of observations or received signal samples. Suppose that we have a signal $\mathbf{X_v}(k)$ in the time domain, and we are collecting the data in a time period of $\mathcal{M}$ multiples of $\mathbf{X_v}(k)$, then the power of the received signal at an antenna branch is equal to $\|\mathcal{M}\sum_k x_v(k)\|^2$ where $x_v(k)$ is the $k$th received signal sample at a single antenna branch. If the noise is random with zero mean and variance equal to $\sigma_\omega^2$, where $\sigma_\omega^2$ is the noise variance applied to the signal $\mathbf{X_v}(k)$, then the noise power is equal to $\mathcal{M}\sigma_\omega^2$ [20]. The signal to noise ratio will be increased by a multiplication factor equal to $\mathcal{M}$. This means that as much the signal observation time increases, as much the SNR increases. In frequency domain, the improvement factor of the gain for the Fast Fourier Transform (FFT) that is applied to the signal $\mathbf{X_v}(k)$ due to increasing the number of samples $\mathcal{M}$ multiples of the signal can be explained. The FFT is considered as a matched filter for a specific frequency passband. It improves the SNR of the examined signal when compressed to the frequency domain [21]. In the following, we will refer signals in frequency domain to suffix $f$. The Fourier transform of the sampled received signal $\mathbf{X_v}(k)$ can be presented as:

$$\mathbf{X_f}(l) = \mathbf{A_v}\mathbf{S_f}(l) + \mathbf{W_f}(l), \quad l = 0,1,2\ldots L-1 \tag{9}$$

where $l = \frac{k\times f_s}{K}$, $f_s$ is the sampling frequency, $\mathbf{X_f}(l)$ the sampled spectrum of the received signal, $\mathbf{S_f}(l)$ the sampled spectrum of the noise free signal $\mathbf{S_v}(k)$, and $\boldsymbol{\omega_f}(l)$ the sampled noise spectrum of $\mathbf{W_v}(l)$. The Fourier transform of the received signal $\mathbf{x_v}(k)$ at specific antenna element is given by:

$$\mathbf{x_f}(l) = \sum_{k=0}^{K-1} x_v(k)\, e^{-j2\pi\frac{l\times k}{K}} \tag{10}$$

where $x_v(l)$ is the $k$th received signal sample. The power spectral density of a received signal according to Perceval's theorem is given by:

$$\mathbf{P_f}(l) = |\mathbf{x_f}(l)|^2 \tag{11}$$

When we are examining a limited frequency band signal from $l_1$ to $l_2$ Hz, the signal power $P_s$ becomes:

$$P_s = 2\sum_{l=l_1}^{l_2} \mathbf{P_f}(l) \tag{12}$$

where $\mathbf{P_f}(l)$ is the power spectrum, and $l_1$ and $l_2$ are the minimum and maximum frequencies in the examined signal, respectively. For AWGN, the noise power spectral density is equal to $N_0/2$. Then the signal to noise ratio can be presented as:

$$\text{SNR} = \frac{2\sum_{l=l_1}^{l_2} \mathbf{P_f}(l)}{N_0/2} \tag{13}$$

If the number of samples is increased by a multiplication factor $\mathcal{M}$, then the signal to noise ratio becomes:

$$\text{SNR} = \frac{2\mathcal{M}^2 \sum_{l=l_1}^{l_2} \mathbf{P_f}(l)}{\mathcal{M} N_0/2} = \mathcal{M} \frac{2\sum_{l=l_1}^{l_2} \mathbf{P_f}(l)}{N_0/2} \tag{14}$$

From Eq. (14), it can be concluded that the signal to noise ratio is increased by a multiplication factor $\mathcal{M}$. Also, we cannot ignore that FFT is applied to a specific length data vector. Sometimes, these data vectors are not periodic which results in high frequency side lobes due to sharp discontinuities in these vectors. Many types of windows can be used to correct these sharp discontinuities effect. On the other hand, the resolution of the FFT output depends on the length of the time window. As an example, the rectangular window has a beam width equal to $\sin(x)/x$ which means that the length of data is inversely proportional to the FFT main lobe width. Increasing data length results in decreasing the main lobe width and so, reducing the noise level and thus improving the resolution. This is another benefit of increasing the observation time. Fig. 2 shows the gain improvement of the FFT output when increasing the number of samples.

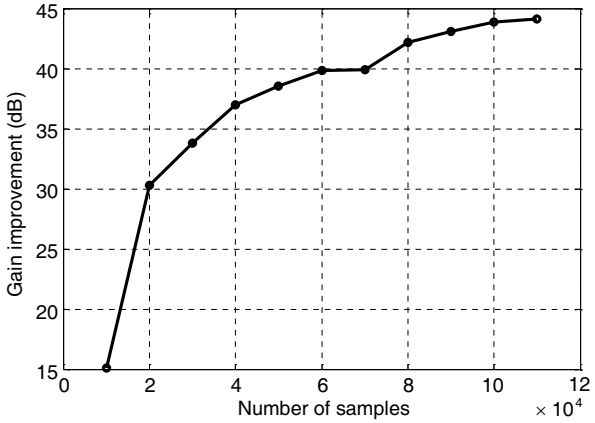


**Figure 2.** Gain improvement at different number of samples.

***Step (3)***: In this step, the singular value decomposition (SVD) of the frequency domain representation of the virtually received signal is performed. The data covariance matrix $\mathbf{R_f}$ using the FFT of the received signal $\mathbf{X_f}(l)$ is given by:

$$\begin{aligned} \mathbf{R_f} &= E\left\{\mathbf{X_f}\mathbf{X_f}^H\right\} = E\left\{\left(\mathbf{A_v}\mathbf{S_f} + \mathbf{W_f}\right)\left(\mathbf{S_f}^H\mathbf{A_v}^H + \mathbf{W_f}^H\right)\right\} \\ &= E\left\{\mathbf{A_v}\mathbf{S_f}\mathbf{S_f}^H\mathbf{A_v}^H\right\} + E\left\{\mathbf{W_f}\mathbf{S_f}^H\mathbf{A_v}^H\right\} + E\left\{\mathbf{A_v}\mathbf{S_f}\mathbf{W_f}^H\right\} + E\left\{\mathbf{W_f}\mathbf{W_f}^H\right\} \end{aligned} \tag{15}$$

where $E\{\,\}$ is the expectation, and $\mathbf{R_f}$ is a square matrix of dimensions $(2M-1)\times(2M-1)$. For uncorrelated signal and noise, the second and third terms are equal zero. Then Eq. (15) can be written as:

$$\mathbf{R_f} = E\left\{\mathbf{A_v}\mathbf{S_f}\mathbf{S_f}^H\mathbf{A_v}^H\right\} + E\left\{\mathbf{W_f}\mathbf{W_f}^H\right\} \tag{16}$$

Let the transmitted signal auto-covariance matrix $\mathbf{R_{sf}} = E\left\{\mathbf{S_f}\mathbf{S_f}^H\right\}$ and the noise auto-covariance matrix $\mathbf{R_{nf}} = E\left\{\mathbf{W_f}\mathbf{W_f}^H\right\}$. Where $[\cdot]^H$ is the hermetian transpose. For $2M-1$ antenna array elements, the data covariance matrix is a $(2M-1)\times(2M-1)$ square matrix and is given by:

$$\mathbf{R_f} = \mathbf{A_v}\mathbf{R_{sf}}\mathbf{A_v}^H + \mathbf{R_{nf}} \tag{17}$$

Using singular value decomposition, the matrix $\mathbf{R_f}$ can be expressed as:

$$\mathbf{R_f} = \mathbf{U_x}\mathbf{\Lambda_x}\mathbf{V_x}^T \tag{18}$$

where $\mathbf{U_x}$ and $\mathbf{V_x}$ are orthogonal matrices such that ($\mathbf{U_x U_x^T = U_x^T U_x = I}$) and ($\mathbf{V_x V_x^T = V_x^T V_x = I}$). The columns of $\mathbf{U_x}$ and $\mathbf{V_x}$ are the left-singular vectors and the right-singular vectors of $\mathbf{R_f}$, respectively.

$\mathbf{\Lambda_x}$ is a diagonal matrix with $\lambda_{ij} = 0 \forall i \neq j$ and $\lambda_{ij} = \lambda_i \geq 0 \forall i = j$, i.e., $\mathbf{\Lambda_x} = \text{diag}(\lambda_1, \lambda_2, \ldots\ldots, \lambda_{2M-1})$, where $(\lambda_1, \lambda_2, \ldots\ldots, \lambda_{2M-1})$ are the eigenvalues of the matrix $\mathbf{R_f}$ in ascending order such that the largest eigenvalue is $\lambda_{\max} = \lambda_{2M-1}$. Let $\bar{\mathbf{u}}$ being the eigenvector corresponding to the largest eigenvalue $\lambda_{\max} = \lambda_{2M-1}$. The $(2M-1) \times 1$ eigenvector $\bar{u}$ can be expressed as:

$$\bar{\mathbf{u}} = (u_1, u_2, \ldots\ldots, u_{2M-1})^T \tag{19}$$

For effective decorrelation of coherent signals, spatial smoothing algorithm is the key solution. In our case, spatial smoothing is performed on the desired $(2M-1)\times 1$ eigenvector $\bar{\mathbf{u}}$ instead of the $M$-elements ULA. It uses the internal relations of adjacent values in the eigenvector $\bar{\mathbf{u}}$ to get the average number of sub-vectors of the smoothed covariance matrix $\mathbf{\Psi}$. The $(2M-1)$ values $u_m$, $m = 1, 2, \ldots\ldots, 2M-1$ of the vector $\bar{\mathbf{u}}$, are divided into $P$ overlapping sub-vectors each of dimensions $L \times 1$, such that $P = (2M-1) - L + 1$ and $L > N$ as clarified in (20).

$$\bar{\mathbf{u}} = \left( \underbrace{u_1, u_2, u_3, u_4, \ldots, u_L}_{1}, u_{L+1}, \underbrace{\ldots, u_{2M-3}, u_{2M-2}, u_{2M-1}}_{P} \right)^T \tag{20}$$

As a result, the $L \times P$ smoothed covariance matrix $\mathbf{\Psi}$ can be expressed as:

$$\mathbf{\Psi} = \begin{bmatrix} u_1 & u_2 & \ldots & u_P \\ u_2 & u_3 & \ldots & u_{P+1} \\ \ldots & \ldots & \ldots & \ldots \\ u_L & u_{L+1} & \ldots & u_{2M-1} \end{bmatrix}_{L \times P} \tag{21}$$

Performing singular value decomposition, the matrix $\mathbf{\Psi}$ can be expressed as:

$$\mathbf{\Psi = U_\Psi \Lambda_\Psi V_\Psi^T} \tag{22}$$

where $\mathbf{U_\Psi}$ and $\mathbf{V_\Psi}$ are the left-singular matrix and the right-singular matrix of $\mathbf{\Psi}$, respectively. If $L > P$, the SVD computes only $P$ eigenvalues of the first $P$ columns of $\mathbf{U_\Psi}$. To avoid this problem, we take $L = M$ and in this case, $P = M$. As a result, $\mathbf{\Lambda_\Psi}$ is a diagonal matrix whose elements are the eigenvalues of $\mathbf{\Psi}$ such that $\mathbf{\Lambda_\Psi} = \text{diag}(\lambda_{\Psi 1}, \lambda_{\Psi 2}, \ldots\ldots, \lambda_{\Psi(M)})$. Here we will define a new parameter denoted as eigenvalue ratio $\epsilon_R$ which equals

$$\epsilon_R = \frac{\textit{maximum eigenvalue}}{\textit{minimum eigenvalue}} = \frac{\lambda_{\Psi 1}}{\lambda_{\Psi(M)}} \tag{23}$$

The minimum eigenvalue mainly corresponds to the noise level contained in the signal while the maximum eigenvalue corresponds to the signal level. Then, as this ratio increases, the signal detection capability increase. To increase the resolution of the SVD, construct the matrix $\mathbf{\Psi_o}$ such that

$$\mathbf{\Psi_o = \Psi \Psi^H} \tag{24}$$

Rewrite (24) using SVD, it can be expressed as:

$$\begin{aligned} \mathbf{\Psi_o} &= \left(\mathbf{U_\Psi \Lambda_\Psi V_\Psi^T}\right) \left(\mathbf{U_\Psi \Lambda_\Psi V_\Psi^T}\right)^H \\ \mathbf{\Psi_o} &= \left(\mathbf{U_\Psi \Lambda_\Psi V_\Psi^T {V_\Psi^T}^H \Lambda_\Psi^H U_\Psi^H}\right) \end{aligned} \tag{25}$$

As $\mathbf{V_\Psi^T}$ is a unitary matrix, then $\mathbf{V_\Psi^T {V_\Psi^T}^H = I}$ and Eq. (25) can be reduced as:

$$\mathbf{\Psi_o} = \left(\mathbf{U_\Psi \Lambda_\Psi \Lambda_\Psi^H U_\Psi^H}\right) \tag{26}$$

Let $\mathbf{\Sigma = \Lambda_\Psi \Lambda_\Psi^H}$, then Eq. (26) can be rewritten as:

$$\mathbf{\Psi_o} = \left(\mathbf{U_\Psi \Sigma\, U_\Psi^H}\right) \tag{27}$$

From Eq. (27) it is noticed that the left-singular matrix of $\mathbf{\Psi_o}$ is still the same as the left-singular matrix of $\mathbf{\Psi}$. While $\mathbf{\Sigma}$ is a diagonal matrix whose elements are the eigenvalues of the new matrix $\mathbf{\Psi_o}$ which

equal the square of the eigenvalues of the matrix $\mathbf{\Psi}$ such that $\mathbf{\Sigma} = \text{diag}(\lambda_{\Psi 1}^2, \lambda_{\Psi 2}^2, \ldots\ldots, \lambda_{\Psi M}^2)$. As a result, the new eigenvalue ratio $\epsilon_{Rnew}$ will equal the square of that of Eq. (24)

$$\epsilon_{Rnew} = \frac{\lambda_{\Psi 1}^2}{\lambda_{\Psi M}^2} = \left(\frac{\lambda_{\Psi 1}}{\lambda_{\Psi M}}\right)^2 = (\epsilon_R)^2 \tag{28}$$

For further performance enhancement, the forward-backward spatial smoothing (FBSS) technique in [22] is applied on the matrix $\mathbf{\Psi_o}$ to construct the smoothed $L \times P$ matrix $\mathbf{\Psi_1}$ which is expressed as:

$$\mathbf{\Psi_1} = \frac{1}{2}\left(\mathbf{\Psi_o} + \mathbf{J_C}\mathbf{\Psi_o^*}\mathbf{J_C}\right) \tag{29}$$

where $\mathbf{\Psi_o^*}$ is the conjugate transpose of $\mathbf{\Psi_o}$ and $\mathbf{J_C}$ is the $(L \times L) = (M \times M)$ exchange matrix which is defined as [22]:

$$\mathbf{J_C} = \begin{bmatrix} 0 & \ldots & 1 \\ \vdots & 1 & \vdots \\ 1 & \ldots & 0 \end{bmatrix}_{L \times L} \tag{30}$$

***Step (4)***: In this step, the estimation of the DOAs of the impinging $N$ signals on the ULA is performed using the spatial spectrum of the Multiple Signal classification (MUSIC) algorithm. Firstly, we should determine both the signal and noise subspaces. Performing SVD for the smoothed matrix $\mathbf{\Psi_1}$, it can be expressed as:

$$\mathbf{\Psi_1} = \left(\mathbf{U_f}\,\mathbf{\Sigma_f}\,\mathbf{V_f^T}\right) \tag{31}$$

where $\mathbf{U_f}$ and $\mathbf{V_f}$ are the left and right singular matrices of $\mathbf{\Psi_1}$, respectively. $\mathbf{\Sigma_f}$ is a diagonal matrix whose elements are the eigenvalues of the matrix $\mathbf{\Psi_1}$ which can be expressed as $\mathbf{\Sigma_f} = \text{diag}(\lambda_{f1}, \lambda_{f2}, \ldots\ldots, \lambda_{fM})$, where $(\lambda_{f1} \leq \lambda_{f2} \leq \ldots\ldots \leq \lambda_{fM})$ are the eigenvalues of the matrix $\mathbf{\Psi_1}$ in ascending order.

To determine the noise subspace $\mathbf{E_n}$ and signal subspace $\mathbf{E_s}$, we define the matrix $\mathbf{U_f}$ as a set of $M \times 1$ eigenvectors $U_{fm}$, $m = 1, 2, 3, \ldots, M$ as follows:

$$\mathbf{U_f} = [U_{f1}\ U_{f2}\ U_{f3}\ \ldots\ U_{fM}] \tag{32}$$

To specify the noise subspace, we should determine the multiplicity $\hat{\rho}$ of the minimum eigenvalue $\lambda_{fm}|_{\min}$. In this case, the estimated number of signals can be given by $\hat{N} = M - \hat{\rho}$. Consequently, the noise subspace $\mathbf{E_n}$ is formed from the eigenvectors corresponding to the smallest $\hat{\rho}$ eigenvalues

$$\mathbf{E_n} = [U_{f1}\ U_{f2}\ \ldots\ U_{f\hat{\rho}}] \tag{33}$$

While the signal subspace $\mathbf{E_s}$ can be defined as follows:

$$\mathbf{E_s} = [U_{f\hat{\rho}+1}\ U_{f\hat{\rho}+2}\ \ldots\ U_{fM}] \tag{34}$$

For higher DOA estimation accuracy, we used the modified MUSIC algorithm introduced in [14] whose spatial spectrum is given by:

$$\boldsymbol{\mathcal{F}}_{\mathbf{music}}(\theta) = \frac{\mathbf{a}^H(\theta)\,\mathbf{\Omega}\,\mathbf{a}(\theta)}{\mathbf{a}^H(\theta)\,\mathbf{E_n}\mathbf{E_n^H}\,\mathbf{a}(\theta)} \tag{35}$$

where $\mathbf{a}(\theta)$ is the steering vector of dimensions $(M \times 1)$ and equals the array factor at angle $\theta$. $\mathbf{\Omega}$ is calculated from the signal subspace $\mathbf{E_s}$ as follows:

$$\mathbf{\Omega} = \mathbf{E_s}\,\mathbf{Q}\,\mathbf{E_s^H} \tag{36}$$

The $\mathbf{Q}$ matrix is calculated from the previously calculated matrix $\mathbf{\Sigma_f} = \text{diag}(\lambda_{f1}, \lambda_{f2}, \ldots\ldots, \lambda_{fM})$ as follows:

$$\mathbf{Q} = \text{diag}\left(\mathbf{\Sigma_{fs}^{-1}} - \sigma_n^2 \times \mathbf{I_N}\right) \tag{37}$$

where $\mathbf{\Sigma_{fs}^{-1}}$ is the inverse of the matrix $\mathbf{\Sigma_{fs}} = \text{diag}(\lambda_{f\hat{\rho}+1}, \lambda_{f\hat{\rho}+2}, \ldots, \lambda_{fM})$ which corresponds to the largest eigenvalues of the matrix $\mathbf{\Sigma_f}$, and $\mathbf{I_N}$ is the $(N \times N)$ identity matrix considering that the estimated number of sources $\hat{N}$ equals the exact number of sources $N$. The number of the largest eigenvalues equals the estimated number of sources $\hat{N} = M - \hat{\rho} \approx N$, while the remaining $\hat{\rho}$ eigenvalues

of the matrix $\mathbf{\Sigma_f}$ are used to construct the matrix $\mathbf{\Sigma_{fn}} = \text{diag}(\lambda_{f1}, \lambda_{f2}, ..., \lambda_{f\hat{\rho}})$. $\sigma_n$ is the average value of the remaining eigenvalues which is given by:

$$\sigma_n = \frac{1}{\hat{\rho}} \text{trace}(\mathbf{\Sigma_{fn}}) \tag{38}$$

## 3. SIMULATION RESULTS

In this section, several simulation scenarios and experimental measurements are performed to verify the effectiveness and superiority of the proposed technique compared to the state of the art DOA estimation techniques. In all scenarios, highly correlated complex signals are utilized in the form:

$$s_n(t) = A_n e^{j2\pi ft+\varphi_n}, \quad n = 1, 2, 3, ... ..., N \tag{39}$$

where $A_n$ and $\varphi_n$ are the signal amplitude and phase, respectively. $f$ is the signal frequency.

### 3.1. Detection of a Few Sources When SNR Is from −20 dB to 0 dB

In this scenario, the performance of the proposed technique is compared with that of the MV-SVD, SVD, VSS, and FBSS DOA estimation techniques over a wide SNR range $-20\,\text{dB} \leq \text{SNR} \leq 0\,\text{dB}$. This is done in light of the assumption that a limited number of $N = 4$ coherent signals impinging on an antenna array consisting of $M = 9$ elements from the directions $\theta_n = -40°$, $-20°$, $10°$ and $20°$. Also, it is assumed that all the signals have the same amplitudes $A_1 = A_2 = A_3 = A_4$, the same frequency, and different phases of $\pi/3$, $\pi/5$, $-\pi/3$, and $-\pi/5$, respectively. The simulation is carried out using $K = 500$ received signal samples. In this case, the received signals are applied to a $K = 500$-points FFT. The down sampling is set to give a single snapshot from each FFT signal, and the data are applied to the SVD analysis and then to the MUSIC algorithm for DOA estimation.

***Test Case 1: DOA Estimation at* SNR = 0 dB**

Figure 3 shows the simulated spatial spectrums of the proposed technique, MV-SVD, SVD, VSS, and FBSS DOA estimation techniques. It is clear that the five techniques highly succeed in detecting the DOAs of the four signals. In addition, it is noticed that the spatial spectrums of the proposed technique and the MV-SVD are matched together. In terms of stability, the five algorithms are applied to the same data 25 times and the results are shown in Figs. 4(a), (b), (c), (d), and (e) for the proposed technique, MV-SVD, SVD, VSS, and FBSS DOA estimation techniques, respectively. It is found that the proposed technique, MV-SVD, and VSS techniques provide much higher stability compared to SVD and FBSS techniques. The instability region of the SVD spectrum around the two angles $\theta_n = 10°$ and $20°$ extends from $2.3°$ to $21.5°$. While the instability region of the FBSS spectrum around the same

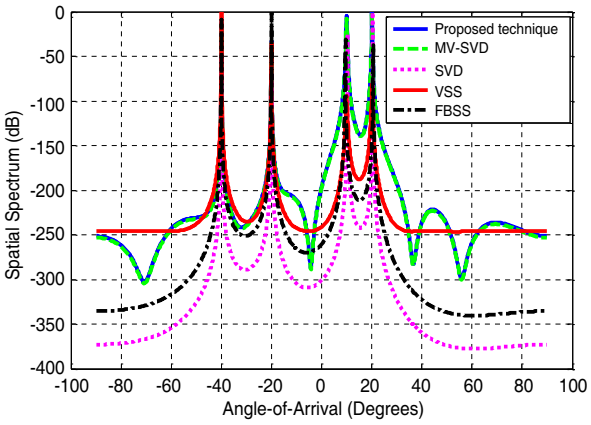


**Figure 3.** The simulated spatial spectrums of the proposed technique, MV-SVD, SVD, VSS, and FBSS techniques at $N = 4$ sources, $M = 9$ elements, $K = 500$ samples, and $\text{SNR} = 0\,\text{dB}$.

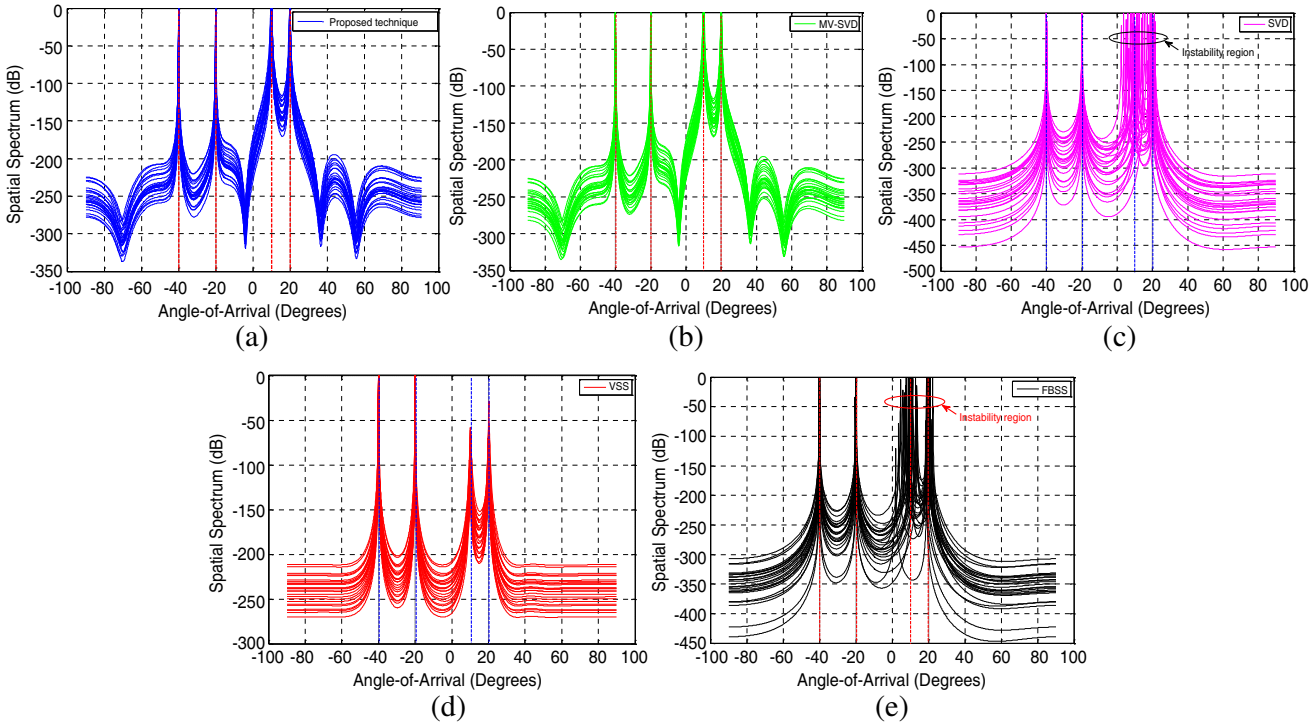


**Figure 4.** Stability test of the (a) proposed technique, (b) MV-SVD, (c) SVD, (d) VSS, and (e) FBSS techniques at $N = 4$ sources, $M = 9$ elements, $K = 500$ samples, and SNR $= 0$ dB.

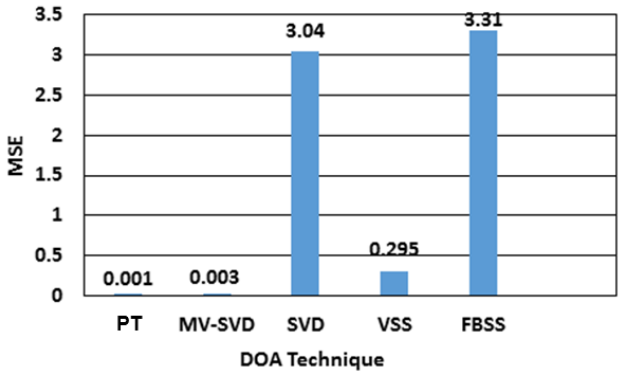


**Figure 5.** The MSE of the proposed technique (PT) compared to the MSE of MV-SVD, SVD, VSS, and FBSS techniques at $N = 4$ sources, $M = 9$ elements, $K = 500$ samples, and SNR $= 0$ dB.

two angles $\theta_n = 10°$ and $20°$ extends from $2°$ to $22.5°$ degrees. This means that the FBSS has less stability than the SVD that results in larger mean square error as shown in Fig. 5. In addition, it is clear that the proposed technique provides lower MSE than the other techniques. Also, in reference to Fig. 4(d), we found that although the VSS technique provides high detection performance, it is noticed that the height of the spectrum peak at the angle $\theta_n = 10°$ is less than $-75$ dB. In practice, this makes it very difficult to detect the source at this angle as it requires a device with very high sensitivity. In contrast, both the proposed technique and the MV-SVD provide high spectrum peaks close to 0 dB at all detected DOAs.

### *Test Case 2: DOA Estimation at* SNR $= -5$ dB

The simulated spatial spectrums of the aforementioned techniques are presented in Fig. 6, and it is

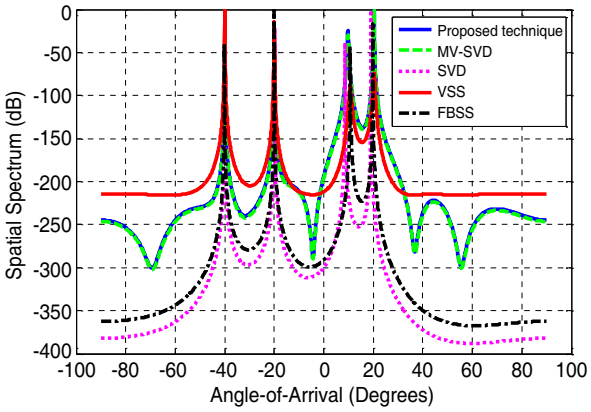


**Figure 6.** The simulated spatial spectrums of the five techniques at $N = 4$ sources, $M = 9$ elements, $K = 500$ samples, and SNR $= -5$ dB.

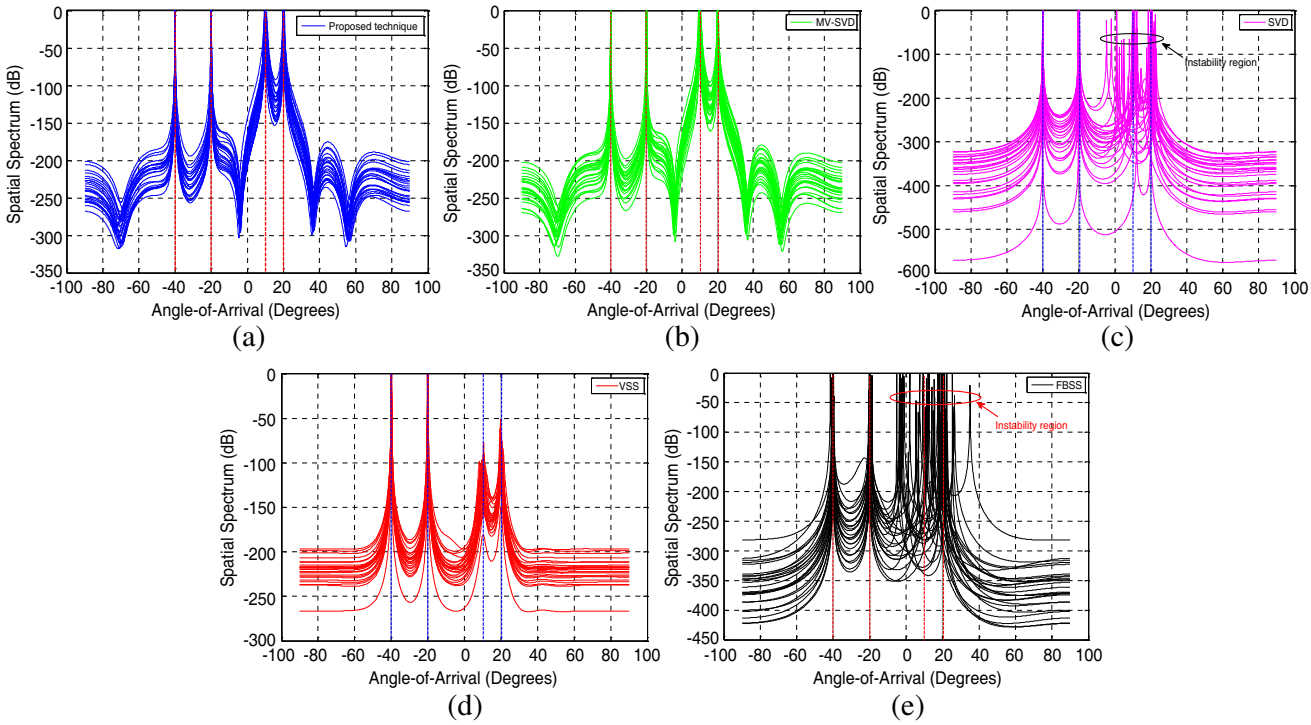


**Figure 7.** Stability test of the (a) proposed technique, (b) MV-SVD, (c) SVD, (d) VSS, and (e) FBSS techniques at $N = 4$ sources, $M = 9$ elements, $K = 500$ samples, and SNR $= -5$ dB.

clear that they succeed in detecting four DOAs of the received signals. It is also noticed that the spatial spectrums of the proposed technique and the MV-SVD are matched together. In terms of stability, it is found that the proposed technique, MV-SVD, and VSS techniques provide higher stability than SVD and FBSS techniques as shown in Fig. 7. The instability regions of the SVD and FBSS spectrums around the two angles $\theta_n = 10°$ and $20°$ extend from $-4.6°$ to $23.2°$ and from $-5.1°$ to $35°$, respectively. Thereby, the FBSS has less stability than the SVD and larger mean square error as shown in Fig. 8. Also, it is clear that the proposed technique provides lower MSE than the other techniques. Regarding the amplitudes of the detected spectrum peaks, the proposed technique and MV-SVD provide high spectrum peaks close to 0 dB at all detected DOAs as shown in Fig. 7, while the VSS technique provides low spectrum peaks of amplitudes less than $-80$ dB at the angle $\theta_n = 10°$.

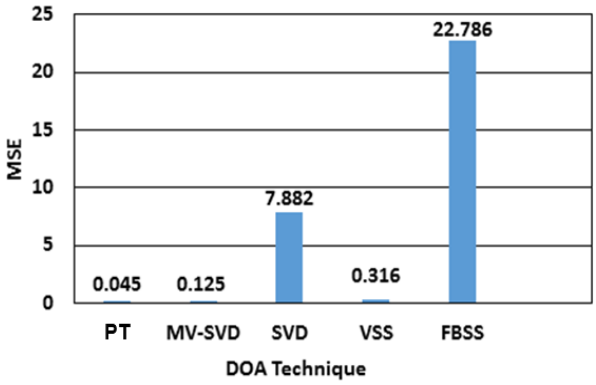


**Figure 8.** The MSE of the proposed technique (PT) compared to the MSE of MV-SVD, SVD, VSS, and FBSS techniques at $N = 4$ sources, $M = 9$ elements, $K = 500$ samples, and SNR $= -5$ dB.

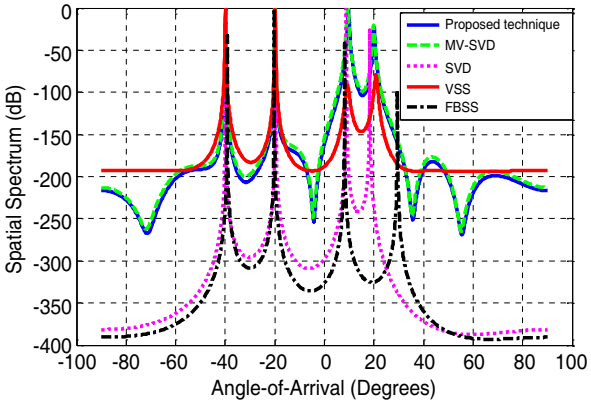


**Figure 9.** The simulated spatial spectrums of the proposed technique, MV-SVD, SVD, VSS, and FBSS techniques at $N = 4$ sources, $M = 9$ elements, $K = 500$ samples, and SNR $= -10$ dB.

### *Test Case 3: DOA Estimation at* SNR $= -10$ dB

As the SNR is lowered to $-10$ dB, more performance degradation occurs in the SVD and FBSS techniques. However, the proposed technique and MV-SVD still have high detection performance with matched spatial spectrums as shown in Fig. 9. The VSS technique also succeeds in detecting the four DOAs, but with spectrum peaks of low amplitudes less than $-70.3$ dB which hinders the practical DOA estimation process as shown in Fig. 10(d). In terms of stability, Fig. 10 shows that the proposed technique and MV-SVD techniques achieve high stability around the intended sources directions. As shown in Fig. 10(d), an instability region appears in the spatial spectrum of the VSS technique around the two angles $\theta_n = 10°$ and $20°$. The instability region of the SVD spatial spectrum around the two angles $\theta_n = 10°$ and $20°$ extend from $-3.2°$ to $26.1°$, while two wide instability regions appear in the spatial spectrum of the FBSS technique extending from $-74°$ to $19.6°$ degrees and from $-6.8°$ to $66°$ for $\theta_n = -40°$ and $-20°$ and $\theta_n = 10°$ and $20°$, respectively. Fig. 11 shows that the proposed technique still has lower MSE than the other techniques.

From the previous simulations, it can be concluded that the proposed technique not only has a superior detection capability but also has higher stability and better MSE performance than the other techniques. Fig. 12 shows the estimated MSEs versus SNR from $-10$ dB to 0 dB for the proposed technique, MV-SVD, SVD, VSS, and FBSS techniques at $N = 4$ sources, $M = 9$ elements, and $K = 500$ samples. The proposed technique has a relatively fixed MSE over the entire SNR range. The MSE of the MV-SVD technique increases very slightly as the SNR decreases, while the MSEs of other techniques significantly increase in proportion to the decay of the SNR, especially the FBSS technique, which achieves the highest MSE.

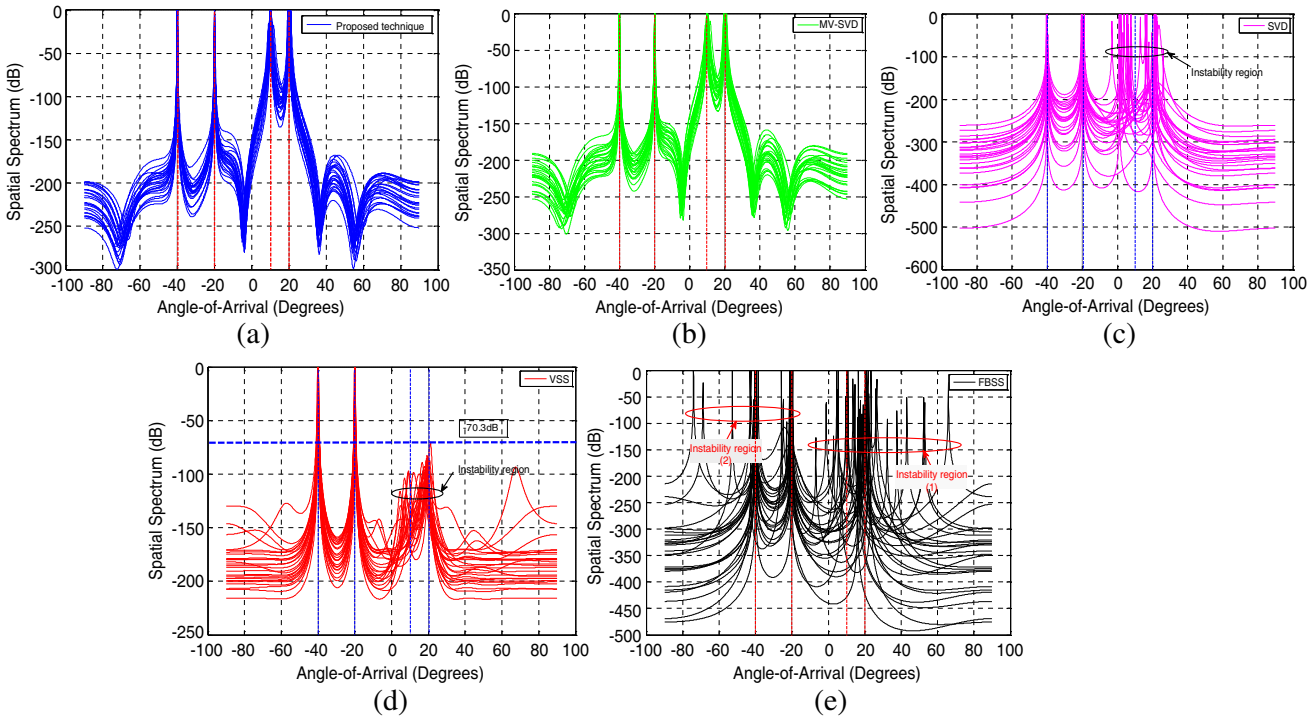


**Figure 10.** Stability test of the (a) proposed technique, (b) MV-SVD, (c) SVD, (d) VSS, and (e) FBSS techniques at $N = 4$ sources, $M = 9$ elements, $K = 500$ samples, and SNR $= -10$ dB.

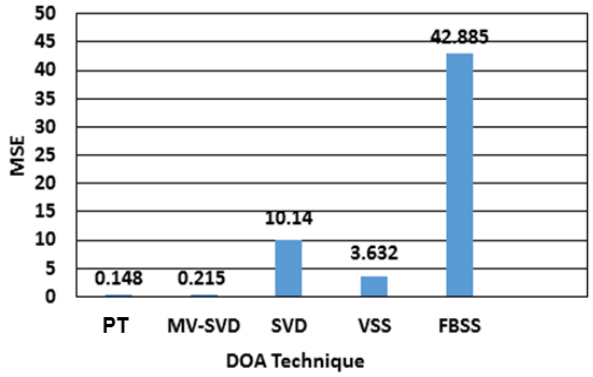


**Figure 11.** The MSE of the proposed technique (PT) compared to the MSE of MV-SVD, SVD, VSS, and FBSS techniques at $N = 4$ sources, $M = 9$ elements, $K = 500$ samples, and SNR $= -10$ dB.

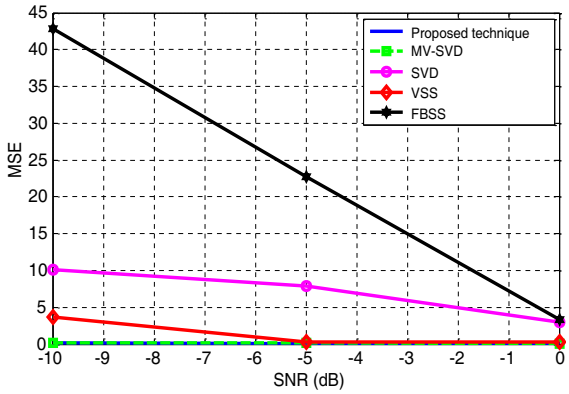


**Figure 12.** The MSE versus SNR for the proposed technique compared to the MSEs of MV-SVD, SVD, VSS, and FBSS techniques at $N = 4$ sources, $M = 9$ elements, and $K = 500$ samples.

### *Test Case 4: DOA Estimation at* SNR $= -20$ dB

To verify the superiority of the proposed technique over other techniques in terms of DOA estimation capability and stability their spatial spectrums are presented as shown in Fig. 13 and Fig. 14, respectively at SNR $= -20$ dB. It is clear that the proposed technique and MV-SVD techniques succeed in detecting the four sources but the proposed technique has sharper spectrum peaks than the MV-SVD technique, while the other techniques fail to detect the four sources.

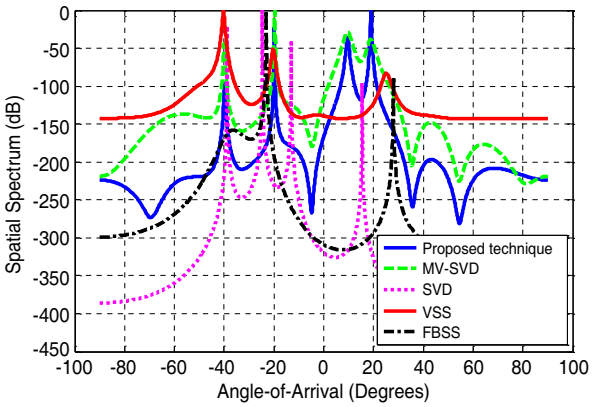


**Figure 13.** The simulated spatial spectrums of the proposed technique, MV-SVD, SVD, VSS, and FBSS techniques at $N = 4$ sources, $M = 9$ elements, $K = 500$ samples, and SNR $= -20$ dB.

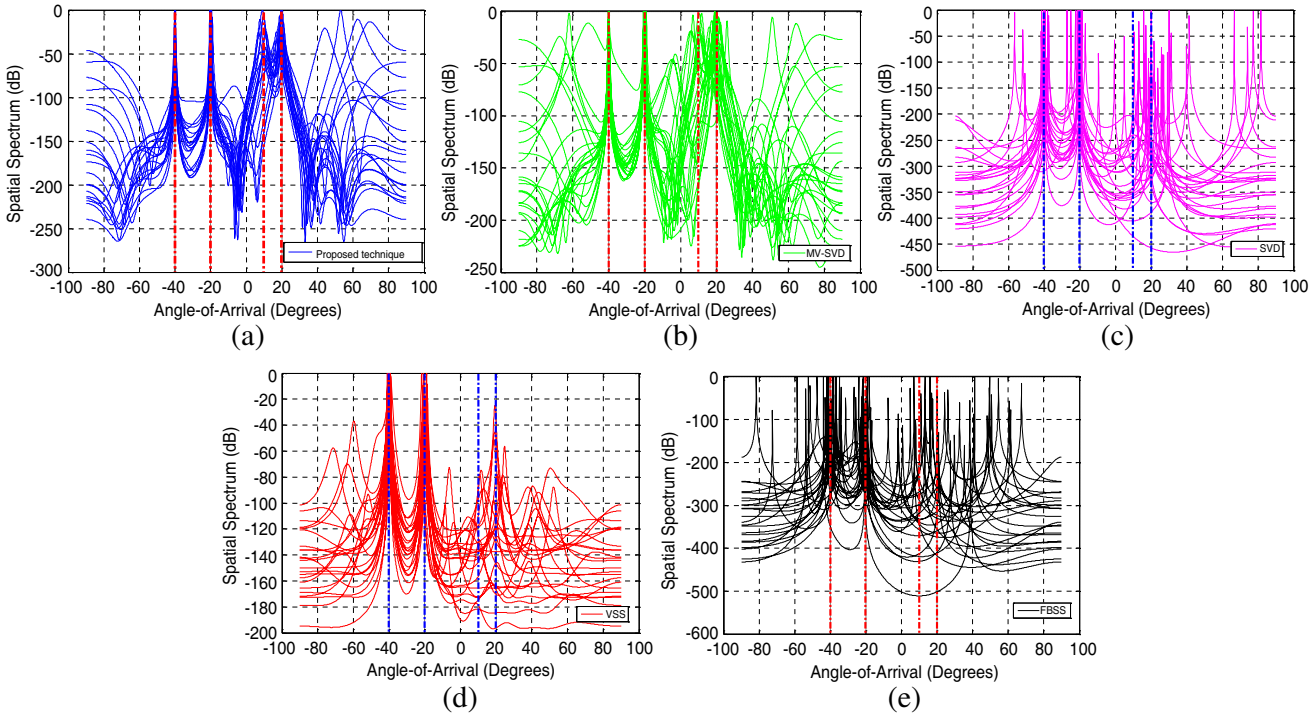


**Figure 14.** Stability test of the (a) proposed technique, (b) MV-SVD, (c) SVD, (d) VSS, and (e) FBSS techniques at $N = 4$ sources, $M = 9$ elements, $K = 500$ samples, and SNR $= -20$ dB.

### 3.2. Detection of Large Number of Sources

In this scenario, the DOA detection capabilities of the proposed technique, MV-SVD, SVD, VSS, and FBSS techniques are tested for $N = 6$ completely coherent signals impinging on the $M = 9$ elements antenna array from the directions $\theta_n = -40°$, $-20°$, $10°$, $20°$, $30°$, and $40°$ at a relatively low SNR $= -10$ dB. The spatial spectrums of these techniques are plotted in Fig. 15 where the proposed technique, MV-SVD, and SVD techniques succeed in detecting the $N = 6$ sources, while the VSS fails to detect one source, and FBSS fails to detect two sources. The simulation revealed the superiority of the proposed technique over the other techniques. It provides the highest accuracy with the lowest MSE $= 0.043$ as listed in Table 1.

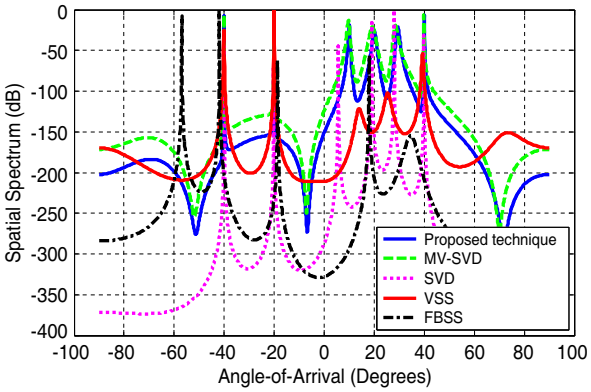


**Figure 15.** The simulated spatial spectrums of the proposed technique, MV-SVD, SVD, VSS, and FBSS techniques at $N = 6$ sources, $M = 9$ elements, $K = 500$ samples, and SNR $= -10$ dB.

**Table 1.** Estimated angels of arrivals and the MSE of the proposed technique, MV-SVD, SVD, VSS, and FBSS techniques for $N = 6$ completely coherent signals coming from the directions $\theta_n = -40°$, $-20°$, $10°$, $20°$, $30°$, and $40°$ at SNR $= -10$ dB.

| $\theta_n$ | $-40°$ | $-20°$ | $10°$ | $20°$ | $30°$ | $40°$ | MSE |
|---|---|---|---|---|---|---|---|
| **Proposed technique** | $-40.1°$ | $-20°$ | $10°$ | $20°$ | $29.5°$ | 40 | 0.043 |
| **MV-SVD** | $-40.1°$ | $-20°$ | $9.7°$ | $19.3°$ | $28.5°$ | 39.8 | 0.48 |
| **SVD** | $-40°$ | $-20.2°$ | $5.6°$ | $19°$ | $28°$ | 39.9 | 4.068 |
| **VSS** | $-40.2°$ | $-20°$ | $13.8°$ | Failed | $25.5°$ | 39.3 | — |
| **FBSS** | $-41.9°$ | $-18.6°$ | Failed | $17.9°$ | $34.2°$ | Failed | — |

### 3.3. Detection of Sources at Very Low SNR $= -35$ dB

In some sensitive applications such as long-range and passive radars, the amplitudes of the received reflections from targets are very small. That led to working under very low SNR regimes. However, the detection of targets in these applications is a vital and indispensable task. Therefore, to achieve a successful detection of targets, we had to use a large number of received signal samples. As an

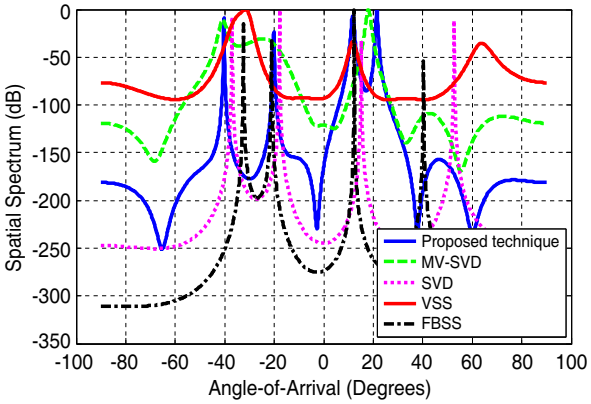


**Figure 16.** The simulated spatial spectrums of the proposed technique, MV-SVD, SVD, VSS, and FBSS techniques at $N = 4$ sources, $M = 9$ elements, $K = 10000$ samples, and SNR $= -35$ dB.

**Table 2.** Estimated angels of arrivals and the MSE of the proposed technique, MV-SVD, SVD, VSS, and FBSS techniques for $N = 4$ completely coherent signals coming from the directions $\theta_n = -40°$, $-20°$, $10°$, and $20°$ at SNR $= -35$ dB.

| $\theta_n$ | $-40°$ | $-20°$ | $10°$ | $20°$ | MSE |
|---|---|---|---|---|---|
| **Proposed technique** | $-40.3°$ | $-20.1°$ | $11.7°$ | $21.3°$ | 1.17 |
| **MV-SVD** | $-41°$ | Failed | Failed | $17.8°$ | — |
| **SVD** | $-37.1°$ | $-17.8°$ | Failed | $15.2°$ | — |
| **VSS** | $-31.6°$ | Failed | $12°$ | Failed | — |
| **FBSS** | $-32.4°$ | $-21.1°$ | $12.3°$ | Failed | — |

example, the performance of the proposed technique is compared to that of the MV-SVD, SVD, VSS, and FBSS techniques at $N = 4$ sources impinging on the $M = 9$ elements antenna array from the directions $\theta_n = -40°$, $-20°$, $10°$ and $20°$, and very low SNR $= -35$ dB. For efficient targets detection, $K = 10000$ samples are used. The down sampling is set to 10000, where the proposed technique uses only a single snapshot. Fig. 16 shows the spatial spectrums of the five techniques, and it is clear that only the proposed technique succeeds in detecting the four sources. The other techniques completely fail to detect these sources. Also the proposed technique provides the lowest MSE as listed in Table 2.

### 3.4. Angular Resolution Test

In this section, the resolution $\Delta_{\theta_{\min}}$ of the proposed technique is evaluated and compared to the resolution of the super-resolution DOA estimation algorithm for correlated signals introduced in [25]. It is based on the hybrid combination between the array signal segregation using an iterative approach (ASSIA) and the closely-spaced nulls synthesis method (CNSM), and it is denoted as the ASSIA-CNSM algorithm. Consider $M = 9$ elements ULA with half power beamwidth HPBW $= 11.34°$, $N = 2$ closely angular spaced coherent signals impinging on the array from the directions $\theta_1 = 10°$ and $\theta_2 = 11°$ with angular spacing $\Delta_\theta = \theta_2 - \theta_1 = 1°$, $K = 2000$ samples, and SNR $= 5$ dB as in [25]. The simulations revealed that the proposed technique succeeds in detecting the DOAs of the two sources at $10°$ and $11.1°$, respectively as shown in Fig. 17. Accordingly, the angular resolution of the proposed technique is $\Delta_{\theta_{\min}} = \left(\frac{\theta_2 - \theta_1}{\text{HPBW}}\right) \times \text{HPBW} = 0.088\text{HPBW}$ while the angular resolution of the ASSIA-CNSM algorithm is $\Delta_{\theta_{\min}} = 0.15\text{HPBW}$.

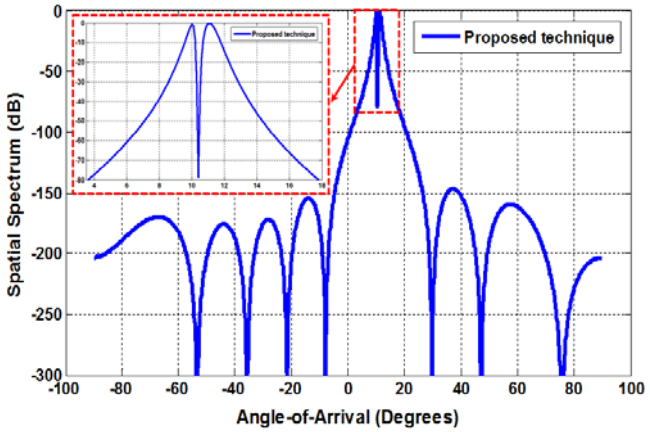


**Figure 17.** The spatial spectrum of the proposed technique for $M = 9$ elements, $N = 2$ coherent sources impinging on the array from the directions $\theta_1 = 10°$ and $\theta_2 = 11°$ with $\Delta_\theta = \theta_2 - \theta_1 = 1°$, $K = 2000$ samples, and SNR $= 5$ dB.

## 4. EXPERIMENTAL DOA ESTIMATION USING AWR1243 MM-WAVE 76–81 GHZ FMCW RADAR

Recently, many real time DOA estimation algorithms are introduced and well experimentally tested in [23–25]. In [23], an experimental DOA estimation using the co-array algorithm is introduced. This algorithm allows the detection of a number of sources larger than the number of available antenna elements. It is applied to three different co-arrays configurations named as nested array (NA), the coprime sampling array (CA), and the sparse ruler array (SRA) and the ULA. The measurements are carried out using thousands of received signal samples at high SNR = 10 dB. In [24], two DOA estimation algorithms named as single/two-port MUSIC algorithm and the power pattern cross correlation (PPCC) algorithm are introduced for real time DOA estimation using reconfigurable leaky-wave antennas (LWAs). The performances of these algorithms are experimentally evaluated, and the measurements show that their performances are highly affected by the multipath propagation and the coupling between antenna elements. In [25], a super resolution DOA estimation algorithm for correlated signals detection using circular antenna arrays is introduced. The experimental measurements show the effectiveness of the algorithm in detecting closely angular spaced sources with angular spacing of (0.15 BW) where BW is the half power beamwidth of the main beam.

In this section, the functionality of the proposed DOA estimation technique is experimentally tested using the AWR1243 mm-wave frequency modulated continuous wave (FMCW) transceiver from Texas Instruments (TI). The AWR1243 device is an integrated single-chip FMCW transceiver capable of operation in the 76- to 81-GHz frequency band. It is built on TI's low-power 45-nm RFCMOS process, which enables a monolithic implementation of a 3 transmit (3TX) and 4 receive (4RX) antenna systems. The AWR1243 device uses MIPI D-PHY/CSI2-based format to transfer the raw ADC samples to the external microcontroller unit (MCU). It supports four data lanes with CSI-2 data rate scalable from 150 Mbps to 600 Mbps per lane. For data capturing from the AWR1243 device, the hardware setup from the AWR1243 EVM, mm-wave DevPack, and TSW1400 EVM is established as shown in Fig. 18. The mm-wave DevPack provides interfaces and PC connectivity to the AWR1243 EVM. It provides an interface for the radar studio tool to configure the AWR1243 radar device and capture the raw ADC data using the TSW1400 EVM capture card. The TSW1400 has two direct interfaces to the AWR1243 ADC EVMs. One option captures the data through an LVDS bus interface providing 16-bits of data at 1.5 GSPS, and the other uses a dual 16-bit CMOS interface. The sampled data from the ADC is de-serialized and formatted by an Altera Stratix IV FPGA, then stored in an external onboard 1 GByte DDR memory card. The onboard memory enables the TSW1400 to store up to 512M 16-bits data samples. To acquire data on a host PC, the FPGA reads the data from memory and transmits it on

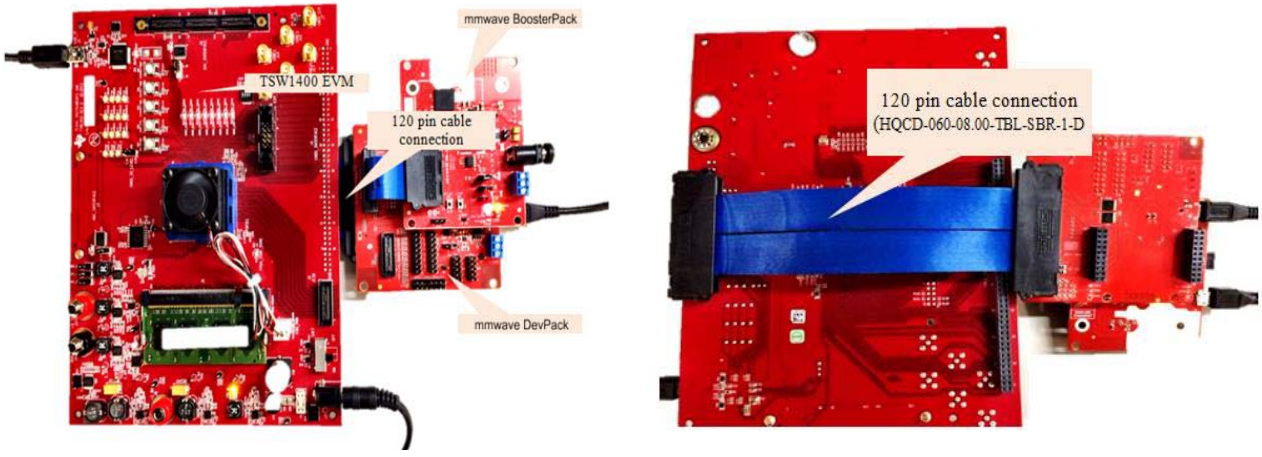


**Figure 18.** AWR1243 EVM board, TSW1400 EVM, and mm-wave DevPack hardware connection of the radar system (a) front view and (b) back view.


**Figure 19.** Experimental setup of the radar system to detect $N = 2$ metallic targets from two different directions $-20°$ and $43°$ at $M = 4$ elements and $K = 256$ samples.

the serial peripheral interface (SPI). An onboard high speed USB to SPI converter bridges the FPGA SPI interface to the host PC. The received data at the host PC is then applied to the proposed DOA estimation program to determine the targets directions of arrivals.

The experimental measurements of the DOAs are performed for $N = 2$ metallic targets placed at equal distances of $L = 2$ meters from the radar system at two different angles $-20°$ and $43°$ as shown in Fig. 19. The reflected signals from the two targets are received by the $M = 4$ receiving antenna elements of the AWR1243 EVM. The element spacing between the receive antenna elements is $d = 1.951\,\text{mm} = \lambda/2$, where $\lambda$ is the wavelength at $f = 76.919\,\text{GHz}$. A set of $K = 256$ complex received signal samples are captured at the same frequency $f = 76.919\,\text{GHz}$ from 256 successive frequency chirps. Fig. 20 shows the measured spatial spectrum of the proposed technique which has two relatively sharp spectrum peaks at $-19.8°$ and $42.8°$. Thus, it can be concluded that the proposed technique practically succeeds in detecting the real targets with very small error MSE $= 0.04°$. The other techniques fail to practically detect the two sources as listed in Table 3.

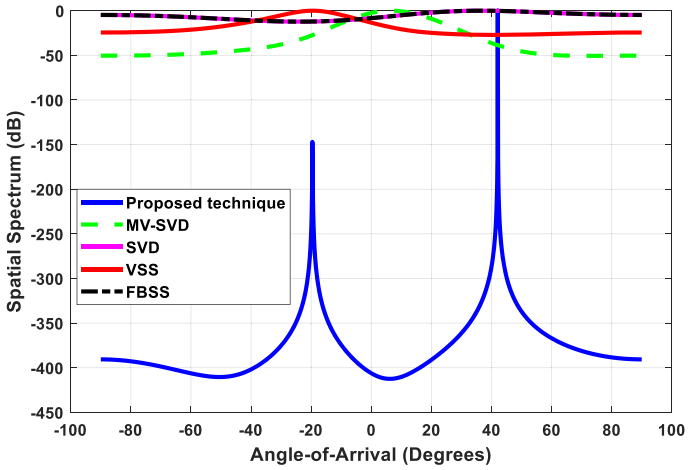


**Figure 20.** Measured spatial spectrums of the proposed technique, MV-SVD, SVD, VSS, and FBSS techniques using the AWR1243 radar system for $N = 2$ metallic targets coming from two different directions $-20°$ and $43°$ at $M = 4$ elements and $K = 256$ samples captured at $f = 76.919\,\text{GHz}$.

**Table 3.** Practical estimation of angels of arrivals using the proposed technique, MV-SVD, SVD, VSS, and FBSS techniques for $N = 2$ completely coherent signals impinging on the $M = 4$ elements receiving array of the AWR1243 radar from the directions $\theta_n = -20^\circ$ and $43^\circ$ and $K = 256$ samples.

| $\theta_n$ | $-20^\circ$ | $43^\circ$ |
|---|---|---|
| **Proposed technique** | $-19.8^\circ$ | $42.8^\circ$ |
| **MV-SVD** | Failed | Failed |
| **SVD** | Failed | $36.5^\circ$ |
| **VSS** | $-19.5^\circ$ | Failed |
| **FBSS** | Failed | $36.5^\circ$ |

## 5. CONCLUSION

In this paper, a highly efficient FFT based DOA estimation technique is introduced. The superiority of the proposed technique distinguishes from combining the FFT algorithm, VAE, SVD, and modified MUSIC techniques to estimate the DOAs of multiple sources. The simulations show that the proposed technique not only has a superior detection capability but also has higher stability and better MSE performance compared to state-of-the-art techniques. Furthermore, it provides a high angular resolution of about 0.088 HPBW that is higher than the state of the art techniques. The proposed technique performance was tested by collecting real data reflected from two targets at the same range and different angles using the AWR1243 radar transceiver. The proposed technique recorded an MSE equal to $0.04^\circ$ with high estimation stability at various experimental trials.

## ACKNOWLEDGMENT

This work is done under the contract between the National telecom regulatory authority (NTRA), Egypt and the electronics research institute in the project entitled "Smart radar system for train collision avoidance and obstacles detection".

## REFERENCES

1. Schmidt, R. O., "Multiple emitter location and signal parameter estimation," *IEEE Transactions on Antennas and Propagation*, Vol. 34, 276–280, Mar. 1986.
2. Zhang, T., "Resarch of modified MUSIC algorithm in DOA estimation of smart antenna," *Journal of Shannxi University of Science and Technology*, Vol. 27, No. 1, 97–101, 2009.
3. Yan, F., M. Jin, and X. Qiao, "Low-complexity DOA estimation based on compressed MUSIC and its performance analysis," *IEEE Trans. Signal Process.*, Vol. 61, 1915–193, 2013.
4. Gardner, W. A., "Simplification of MUSIC and ESPRIT by exploitation of cyclostationarity," *Proc. IEEE*, Vol. 76, 845–847, 1988.
5. Roy, R. and T. Kailath, "ESPRIT-estimation of signal parameters via rotational invariance techniques," *IEEE Transactions on Acoustics, Speech, and Signal Processing*, Vol. 37, 984–995, Jul. 1989.
6. Cui, H., Y. Qian, and D. Li, "Direction of arrival research on extracting signal subspace of ESPRIT algorithm," *Compute Engineering and Design*, Vol. 30, No. 13, 3057–3059, 2009.
7. Rao, B. D. and K. V. S. Hari, "Effect of spatial smoothing on the performance of MUSIC and the minimum-norm method," *IEEE Proceedings*, Vol. 137, No. 6, 449–458, Dec. 1990.
8. Williams, R., S. Prasad, and A. K. Mahalanbis, "An improved spatial smoothing technique for bearing estimation in a multipath environment," *IEEE Transactions on Acoustics, Speech, and Signal Processing*, Vol. 36, No. 4, 425–432, Apr. 1988.

9. Duan, H., D. Huang, L. Zhou, H. Chen, and J. Shi, "A decorrelation algorithm based on virtual array extension," *7th International ICST Conference on Communications and Networking in China (CHINACOM)*, 348–351, 2012.
10. Kim, B., S. Kim, and J. Lee, "A novel DFT-based DOA estimation by a virtual array extension using simple multiplications for FMCW radar," *Sensors*, Vol. 18, 1560, 2018.
11. Zhang, J., D. Huang, P. Huang, and J. Kang, "Estimation DOAs of the coherent sources based on SVD," *2nd International Conference on Signal Processing Systems (ICSPS)*, Vol. 3, 174–177, 2010.
12. Zhou, L., D. Huang, H. Duan, and Y. Chen, "A modified ESPRIT algorithm based on a new SVD method for coherent signals," *Proceeding of the IEEE International Conference on Information and Automation*, 75–78, Shenzhen, China, Jun. 2011.
13. El-Barbary, K. A., T. S. Mohamed, and M. S. Melad, "High resolution direction of arrival estimation (coherent signal source DOA estimation)," *International Journal of Engineering Research and Applications (IJERA)*, Vol. 3, No. 1, 132–139, 2013.
14. El Dosouky, B., A. H. Hussein Abdullah, and S. Khamis, "A new high-resolution and stable MV-SVD algorithm for coherent signals detection," *Progress In Electromagnetics Research M*, Vol. 35, 163–171, 2014.
15. Wang, P., Y. Kong, X. He, M. Zhang, and X. Tan, "An improved squirrel search algorithm for maximum likelihood DOA estimation and application for MEMS vector hydrophone array," *IEEE Access*, Vol. 7, 118343–118358, 2019.
16. Reddy, V. V., M. Mubeen, and B. P. Ng, "Reduced-complexity super-resolution DOA estimation with unknown number of sources," *IEEE Signal Processing Letters*, Vol. 22, No. 6, 772–776, Jun. 2015.
17. Ying, Z. and B. P. Ng, "Music-like DOA estimation without estimating the number of sources," *IEEE Trans. Signal Process.*, Vol. 58, No. 3, 1668–1676, 2010.
18. Hussein Abdullah, A. H., "A new GE/PSO antenna arrays synthesis technique and its application to DOA estimation," *Progress In Electromagnetics Research M*, Vol. 56, 43–52, 2017.
19. Hussein, A. H., H. H. Abdullah, A. M. Salem, S. Khamis, and M. Nasr, "Optimum design of linear antenna arrays using a hybrid MoM/GA algorithm," *IEEE, Antennas and Wireless Propagation Letters*, Vol. 10, 1232–1235, Oct. 2011.
20. Rangayyan, R. M., *Biomedical Signal Analysis, A Case-study Approach*, Wiley-Interscience, New York, 2002.
21. Johnson, D. H., *Fundamentals of Electrical Engineering I*, Rice University, Houston, Connexions, 2013.
22. Pillai, S. U. and B. H. Kwon, "Forward-backward and spatial smoothing techniques for the coherent signal identification," *IEEE Transactions on Acoustics, Speech, and Signal Processing*, Vol. 37, No. 1, 8–15, 1989.
23. Wang, J., H. Xu, G. J. T. Leus, and G. A. E. Vandenbosch, "Experimental assessment of the coarray concept for DoA estimation in wireless communications," *IEEE Transactions on Antennas and Propagation*, Vol. 66, No. 6, 3064–3075, Jun. 2018.
24. Paaso, H., et al., "DoA estimation using compact CRLH leaky-wave antennas: Novel algorithms and measured performance," *IEEE Transactions on Antennas and Propagation*, Vol. 65, No. 9, 4836–4849, Sep. 2017.
25. Amjadi, S. M. and K. Sarabandi, "Super resolution DoA estimation with circular arrays using signal segregation algorithm in conjunction with a nulls-synthesis method," *IEEE Transactions on Antennas and Propagation*, Vol. 66, No. 6, 3108–3121, Jun. 2018.